Appl Phys A (2009) 94: 167–171
DOI 10.1007/s00339-008-4721-x

Applied Physics A
Materials Science & Processing

Calculations of electronic structure and density of states in the wurtzite structure of $Zn_{1-x}Mg_xO$ alloys using sp^3 semi-empirical tight-binding model

Kuo-Feng Lin · Ching-Ju Pan · Wen-Feng Hsieh

Received: 2 January 2008 / Accepted: 22 May 2008 / Published online: 21 June 2008

Abstract Calculating the electronic structure and the density of states in the wurtzite structure of $Zn_{1-x}Mg_xO$ (ZMO) alloys using sp^3 semi-empirical tight-binding model, we observed increases of both band gap and electron effective mass that agree with the experimental results as increasing Mg composition up to $x = 0.3$. From the calculated total density of states, the increasing electron effective mass is a result of less orbital overlap of cation sites due to extra density of modes coming from Mg3s and Mg3p orbitals as introducing more Mg composition. Additionally, reducing electronegative characteristic of oxygen was caused by that the O2p was less localized around the oxygen atom.

PACS 71.20.-b · 71.55.Gs · 74.25.Jb · 71.20.Nr · 87.15.Pc

1 Introduction

In the past decade, the advantageous technologies of light-emitting diodes (LED) and semiconductor lasers realize full-color display systems which have prompted the research for devices operating in the blue-ultraviolet (UV) [1–3]. Zinc-oxide (ZnO) materials have drawn considerable attention for the application in UV optoelectronics because of their excitonic transition energy (∼3.37 eV) and large exciton binding energy (∼60 meV). The band gap becomes even larger if Zn atoms are substituted by magnesium (Mg) atoms, which have a similar ionic radius, allowing for quantum-well structures and superlattices [4–6]. The change of band gap of the $Zn_{1-x}Mg_xO$ (ZMO) layers grown on sapphire [21] with $0.1 < x < 0.3$ and powders [20] with $0 < x < 0.05$ have been reported; and in the Al doped ZMO alloys with a preferential c-axis orientation, Lu et al. [23] experimentally showed that the electron effective masses increase with increasing Mg concentration. However, it is still lack of theoretical confirmation of bandgap and electron effective mass as increasing Mg incorporation.

In the wurtzite $Zn_{1-x}Mg_xO$ (ZMO) alloys, Malashevich et al. [28] investigated the polarization-related properties based on density-functional-theory calculation under the local-density approximation and the Berry-phase approach to calculate electric polarization. Li and Wei [25] used the first-principle band-structure method to show that if Mg atoms substitute Zn atoms to reduce the anion and cation kinetic p-d repulsion, the acceptor transition energy of N_O–nZn_{Zn} can be reduced. Whereas, the application of the first-principles calculation to study electronic band structure of disordered alloys and solid solutions generally requires using very large supercell in order to mimic the distribution of local chemical environments. It is very computationally demanded. On the other hand, the tight-binding (TB) theory is a versatile and simple method to calculate the electronic properties of solids. Additionally, due to the transferability of the TB parameters, the method has been readily applied to systems with broken translational invariance such as low-dimensional structures, clusters, and alloys. Using the TB approach, among the quantities that are successfully calculated, there are elastic constants [7], phonon spectra [8], vacancy-formation energies, and surface energies [9, 10], as well as cluster-formation [11] energies and magnetic moments. Particularly, the electronic structure of semiconductor compounds is well calculated in the complete Brillouin zone [12, 13]. Additionally, the tight binding method gives reliable results for bands originating from

Kuo-Feng Lin · Ching-Ju Pan · Wen-Feng Hsieh (✉)
Department of Photonics and Institute of Electro-Optical Engineering, National Chiao Tung University, 1001 Tahsueh Rd., Hsinchu 30050, Taiwan
e-mail: wfhsieh@mail.nctu.edu.tw

well-localized atomic states. ZnO and MgO are both ionic semiconductors; therefore, the tight binding model should be also suitable for studying ZMO compound semiconductors. Nevertheless, there were few theoretically calculations of the electronic structure in the $Zn_{1-x}Mg_xO$ alloy system. Particularly, for electronic devices, knowledge of the effective masses is especially important for analyzing the device properties, especially the current transport characteristics.

In this letter, we present the electronic band structure and total density of states (DOS) of ZnO and ZMO alloy crystallization using the nearest- and the next-nearest-neighbor semi-empirical tight-binding (SETB) approach sp^3 model [14].

2 Theoretical details

We present the electronic band structure and total DOS of ZnO and ZMO alloy crystallization using the nearest- and the next-nearest-neighbor semi-empirical tight-binding (SETB) approach sp^3 model [14], which has proven its capability in the case of bulk wurtzite crystals. The virtual-crystal approximation (VCA) [12] treats an alloy as a perfectly periodic crystal by assuming the symmetry of the constituents being identical to the symmetry of pure crystal. In the compound $Zn_{1-x}Mg_xO$ semiconductor, a virtual atom, whose wavefunctions of electrons are linear combinations of atomic orbitals of the constituent Zn and Mg atoms, is assumed to occupy the cation site in a unit cell, while anion site is occupied by O atom. Therefore, the effect of disorder is absent in our results. However, in order to ensure the virtual crystal approximation is valid, the ZMO alloy must keep with the wurtzite structure. The wurtzite ZMO alloy is stable with respect to the corresponding rocksalt alloy for $x < 0.375$ [17, 18]. The VCA was used by taking weighted averages of the diagonal matrix elements for the band structures of the alloys, namely, we write the SETB parameters of the binary compounds,

$$E_b(Zn_{1-x}Mg_xO) = (1-x)E_b^{ZnO} + xE_b^{MgO},$$
$$b = s, p_x, p_y, p_z, \quad (1)$$

where $E_b^{ZnO,MgO}$ are the binding energies of corresponding orbitals of Zn and Mg bound to O2p and O2s orbitals, and x is the incorporation concentration of Mg. The off-diagonal matrix elements, multiplied by the square of the bond length, are also averaged this way (Harrison's rules) [15] with the bond length obtained from Vegard's law [16],

$$d(Zn_{1-x}Mg_xO) = (1-x)d_{ZnO} + xd_{MgO}. \quad (2)$$

All the parameters are listed in Table 1. The VCA treats an alloy as a perfectly periodic crystal, assuming its symmetry identical to the symmetry of the constituents; therefore, it does not describe the different local atomic environment in inhomogeneous materials and has failed in unusual semiconductors [29]. However, the VCA has the advantage of simplicity and computational efficiency, and this approach also has been successfully to solve problems about structure, thermodynamics, dielectric, and piezoelectric properties of some materials [30, 31].

Table 1 Tight-binding parameters of ZnO and MgO alloys (in eV)

	ZnO	MgO
$E(s,a)$	−19.046	−20.02
$E(p,a)$	4.142	4.2
$E(s,c)$	1.805	1.753
$E(p,c)$	12.368	12.1986
$V(s,s)$	−6.043	−6.89289
$V(x,x)$	7.157	8.16356
$V(x,y)$	10.578	12.0657
$V(sa,pc)$	4.703	5.36443
$V(pa,sc)$	8.634	9.84829
λ_a	0.032	0.032
λ_c	0.085	0.0074

3 Results and discussion

3.1 Band structures of $Zn_{1-x}Mg_xO$

The resultant band structures for ZnO and $Zn_{0.7}Mg_{0.3}O$ are given in Fig. 1. The deepest and lowest valence band of ZnO crystal (Fig. 1a) near −20 eV corresponds to an atomic-like O2s state, and the upper valence bands are mainly composed of the O2p state and Zn4s and 4p states. The lowest conduction band is contributed by Zn4s state, and the uppermost conduction bands are primarily caused by Zn4p character. The ZMO is direct band gap semiconductor for all stable wurtzite structures and has band gap ranging from 3.429 eV for ZnO to 4.153 eV for $Zn_{0.7}Mg_{0.3}O$. In addition, we also estimate the p-doubly degeneracy in valence bands with renormalized atomic spin–orbital (SO) splitting of the anion and cation p states [19]. For ZnO we got 15 meV for SO energy (Δ_0), offering a good agreement with experimental results [20], while the modification of SO energy was not conspicuously observed in $Zn_{1-x}Mg_xO$ alloy. However, we perceived that the band gap at Γ point increases as Mg concentration increases.

3.2 Energy gaps and effective masses

In Fig. 2 we plotted the change of the band gaps at Γ points of ZMO alloys as a function of the Mg mole fraction x along with the experimental results from the ZMO layers grown

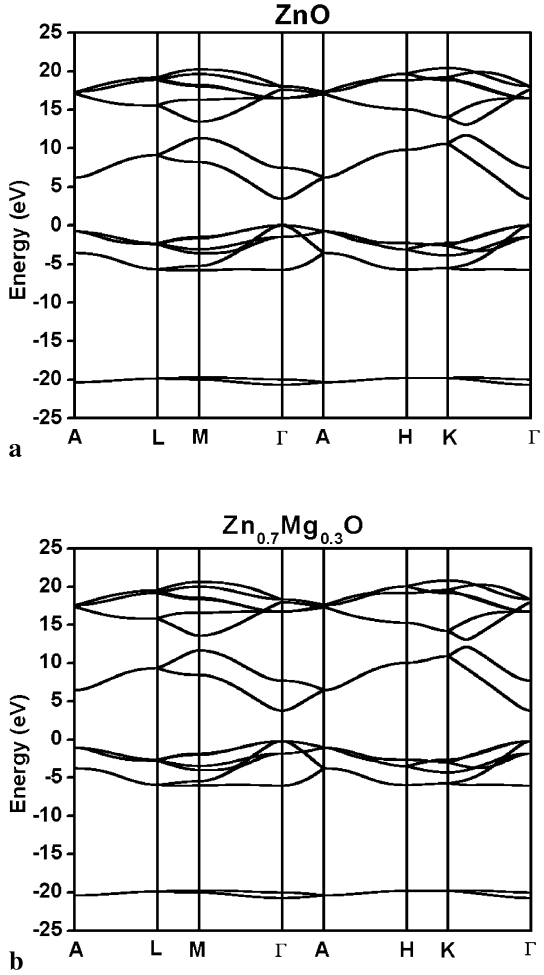

Fig. 1 Calculated band structure of (**a**) ZnO and (**b**) $Zn_{0.7}Mg_{0.3}O$ using semi-empirical tight-binding model

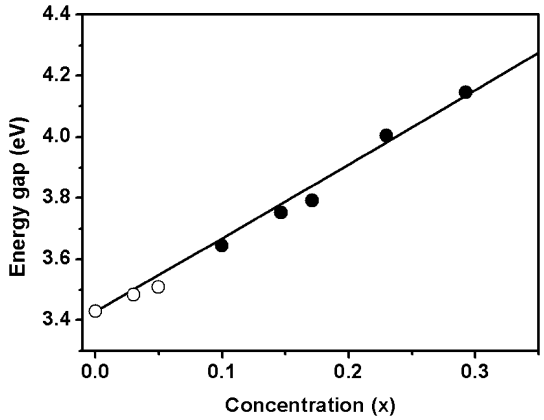

Fig. 2 The energy gaps of wurtzite $Zn_{1-x}Mg_xO$ alloys as a function of Mg mole fraction x. The *hollow circles* and *solid circles* show experimental data from Refs. [20, 21]

on sapphire (solid circle point) [21] and powders (hollow circle point) [20] in the range $0 < x < 0.30$. It shows very good agreement of our calculated curve with the experimental results that the band gap increases with increasing Mg concentration. The curves can be fitted by the polynomials

$$E_g^{\Gamma} = 3.429 + 2.377x + 0.1349x^2 \text{ (eV)}, \tag{3}$$

although the quadratic term is referred as the band-gap bowing factor being 0.1349, which depends on the substrate on which the layer was grown [22].

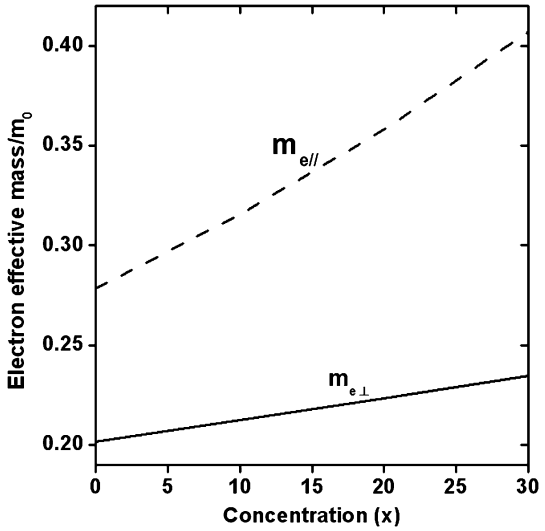

Fig. 3 Composition dependence of the electron effective masses. The *dash line* shows the electron effective mass parallel to the c-axis, and the *solid line* is for perpendicular to the c-axis

The effective mass is given by the curvature of the dispersion relation $E(\boldsymbol{k})$ according to $(\frac{1}{m^*})_{\mu\nu} = \frac{1}{\hbar^2}\frac{d^2E(k)}{dk_\mu\, dk_\nu}$, where $\boldsymbol{k}$ is the wave vector of electron in the crystal, and μ and ν are Cartesian coordinates. Figure 3 shows the calculated effective masses for the alloys ZMO as a function of Mg concentration x. We found that the electron effective mass increases when the Mg concentration increases. In ZnO wurtzite structure ($x = 0$), the electron effective masses of the lowest conduction band for parallel and perpendicular to the c-axis are $m_e^{\parallel} = 0.278m_0$ and $m_e^{\perp} = 0.202m_0$, respectively. These values agree well with experimental data of Button et al. [26] determined from the cyclotron resonance measurements. As aforementioned, the lowest conduction band is mainly caused by Zn4s state; the electron effective masses are mainly determined by the overlapping wavefunctions of s-orbital among cation sites. Lu et al. [23] also observed the same results from the modified Burstein–Moss model in the Al doped ZMO alloys with a preferential c-axis orientation. They indicated that the electron effective masses increase with increasing Mg concentration, while the carrier mobility and electron concentration decrease. Furthermore, we note that variation of electron effective masses is more obvious for $m_e^{\parallel}$ than for $m_e^{\perp}$ in the ZMO alloys. Since the ZnO has wurtzite structure and the MgO is cubic, the lattice along c-axis changes more dramatically than that along a-axis as more Mg atoms substituting Zn atoms.

3.3 Density of states

We calculated the total DOS of ZMO alloys by summation over all bands using a Gaussian function with a broadening parameter of 0.01 eV, e.g., due to temperature broadening around 77 K. As shown in Fig. 4, we obtained the similar DOS for the concentration ranging from 0 to 10%, while the DOS of upper valence bands were slightly broadened and decreased as increasing Mg incorporation. Imai et al. [24] used the first-principle pseudopotential method to show that the bond of Zn–O is more ionic than Zn–S due to the probability of electron lingering between Zn and O is much smaller than between Zn and S. Similar to those obtained by Li et al. [25] using the first-principle calculation, the increasing probability of electron lingering between cation and anion with increasing Mg composition suggest that in the ZMO alloys the electrons from O2p orbital are less localized around the oxygen atom to cause reduction of electronegative characteristic of oxygen and ionization energy of acceptors.

As shown in Figs. 4c and d, we found both the DOS of the upper valence band near −2.7 eV and the uppermost conduction bands near 19 eV increase as Mg composition increases. Because the weighting of Mg's atomic orbital increases with increasing Mg concentration in the VCA method, we believe that the Mg3s orbital mainly contributes extra density of modes to the upper valence band, and the Mg3p orbitals principally contribute extra density of modes to the uppermost conduction bands. Additionally, the DOS of the near lowest conduction band increases with more localized wavefunction as increasing Mg incorporation. Since the orbital energy of Mg3s is lower than that of Zn4s [27], the overlapping integral among cation sites reduces, and consequently, the less overlap of wavefunctions of the neighboring cation atoms results in narrowing the width of conduction band so that the larger effective mass. The wavefunction overlapping determines the rate of quantum tunneling of an electron from one ion to another so that the electrons hop slower from one ion to an adjacent one in the lattice with increasing Mg concentration that shows the larger effective electron mass.

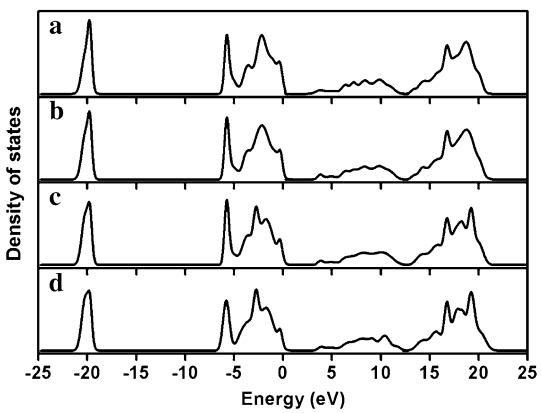

Fig. 4 Total density of states of various Mg concentrations in the wurtzite $Zn_{1-x}Mg_xO$ alloys: (**a**) 0%, (**b**) 10%, (**c**) 20%, and (**d**) 30%

4 Conclusion

In conclusion, using sp^3 semi-empirical tight-binding model under virtual-crystal approximation, we have calculated the electronic band structure and the total density of states for the wurtzite structure of $Zn_{1-x}Mg_xO$ alloys semiconductor. We observed enlarging band gap and increasing electron effective mass that agree with the experimental results as increasing Mg composition up to $x = 0.3$. From the calculated total density of states, due to extra density of modes coming from Mg3s and Mg3p orbitals as introducing more Mg composition, the increasing electron effective mass is a result of less orbital overlap of cation sites. In addition, the O2p is less localized around the oxygen atom to cause reducing electronegative characteristic of oxygen.

Acknowledgements This work was partially supported by the National Science Council and the Ministry of Economic of the Republic of China under Contract No. NSC-96-2628-M009-001-MY3.

References

1. H.D. Sun, T. Makino, Y. Segawa, M. Kawasaki, A. Ohtomom, K. Tamura, H. Koinuma, J. Appl. Phys. **91**, 1993 (2002)
2. C.J. Pan, K.F. Lin, W.F. Hsieh, Appl. Phys. Lett. **91**, 111907 (2007)
3. D.B. Yao, Y.F. Chan, N. Wang, Appl. Phys. Lett. **81**, 757 (2002)
4. E.S. Jang, J.Y. Bae, J. Yoo, W.I. Park, D.W. Kim, G.C. Yi, T. Yatsui, M. Ohtsu, Appl. Phys. Lett. **88**, 023102 (2006)
5. T. Makino, C.H. Chia, N.T. Tuan, H.D. Sun, Y. Segawa, M. Kawasaki, A. Ohtomom, K. Tamura, H. Koinuma, Appl. Phys. Lett. **77**, 975 (2000)
6. P. Misra, T.K. Sharma, S. Porwal, L.M. Kukreja, Appl. Phys. Lett. **89**, 161912 (2000)
7. Q. Zhao, M.B. Nardelli, J. Bernholc, Phys. Rev. B **65**, 144105 (2002)
8. F. Cleri, V. Rosato, Phys. Rev. B **48**, 22 (1993)
9. I. Shalish, H. Temkin, V. Narayanamurti, Phys. Rev. B **69**, 245401 (2004)
10. T. Akiyama, K. Nakamura, T. Ito, Phys. Rev. B **73**, 235308 (2006)
11. S. Sapra, D.D. Sarma, Phys. Rev. B **69**, 125304 (2004)
12. D.W. Jenkins, J.D. Dow, Phys. Rev. B **39**, 3317 (1989)
13. H.H. Cocoletzi, D.A. Contreras, J. Arriaga, Appl. Phys. A **81**, 1029 (2005)
14. A. Kobayashi, O.F. Sankey, S.M. Volz, J.D. Dow, Phys. Rev. B **28**, 935 (1983)
15. W.A. Harrison, *Electronic Structure and he Properties of Solids* (Freeman, San Francisco, 1980), p. 47
16. L. Vegard, Z. Phys. **5**, 17 (1921)
17. Y.-S. Kim, E.-C. Lee, K.J. Chang, J. Korean Phys. Soc. **39**, S92 (2001)
18. M. Sanati, G.L.W. Hart, A. Zunger, Phys. Rev. B **68**, 155210 (2003)
19. D.J. Chadi, Phys. Rev. B **16**, 790 (1977)

20. C.J. Pan, K.F. Lin, W.F. Hsieh, J. Appl. Phys. **102**, 123504 (2007)
21. R. Schmidt, B. Rheinländer, M. Schubert, D. Spemann, T. Butz, J. Lenzner, E.M. Kaidashev, M. Lorenz, A. Rahm, H.C. Semmelhack, M. Grundmann, Appl. Phys. Lett. **82**, 2260 (2003)
22. A.F. Wright, J.S. Nelson, Appl. Phys. Lett. **66**, 3051 (1995)
23. J.G. Lu, S. Fujita, T. Kawaharamura, H. Nishinaka, Y. Kamada, T. Ohshima, Appl. Phys. Lett. **89**, 262107 (2006)
24. Y. Imai, A. Watanabe, I. Shimono, J. Mater. Sci. Mater. Electron. **14**, 149 (2003)
25. J. Li, S.H. Wei, S.S. Li, J.B. Xia, Phys. Rev. B **74**, 081201 (2006)
26. K.J. Button, D.R. Cohm, M. von Ortenverger, B. Lax, E. Mollwo, R. Helbig, Phys. Rev. Lett. **28**, 1637 (1972)
27. E. Chementi, C. Roetti, At. Data Nucl. Table **14**, 177 (1972)
28. A. Malashevich, D. Vanderbilt, Phys. Rev. B **75**, 045106 (2007)
29. C. Chen, E.G. Wang, Y.M. Gu, Phys. Rev. B **57**, 3753 (1998)
30. S. de Gironcoli, P. Giannozzi, S. Baroni, Phys. Rev. Lett. **66**, 2116 (1991)
31. L. Bellaiche, D. Vanderbilt, Phys. Rev. B **61**, 7877 (2000)